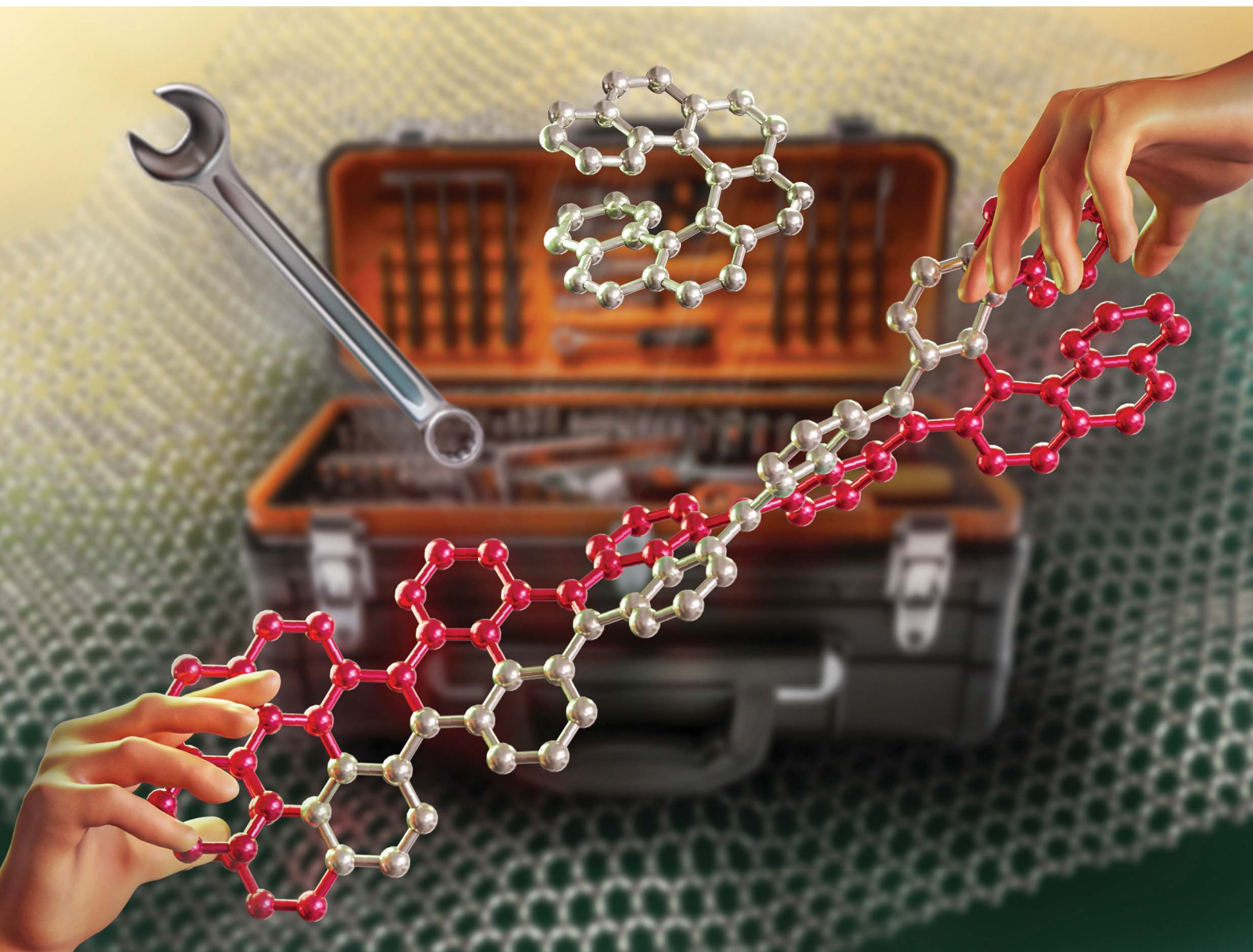


# Chemical Science

Volume 15  
Number 30  
14 August 2024  
Pages 11669–12150

rsc.li/chemical-science



ISSN 2041-6539

**EDGE ARTICLE**





Prince Ravat *et al.*

Helically twisted nanoribbons *via* stereospecific annulative  $\pi$ -extension reaction employing [7]helicene as a molecular wrench

Cite this: *Chem. Sci.*, 2024, 15, 11737

All publication charges for this article have been paid for by the Royal Society of Chemistry

# Helically twisted nanoribbons *via* stereospecific annulative $\pi$ -extension reaction employing [7]helicene as a molecular wrench†

Asim Swain, <sup>a</sup> Krzysztof Radacki, <sup>b</sup> Holger Braunschweig <sup>b</sup> and Prince Ravat <sup>\*a</sup>

Over the past decade, significant progress has been made in synthesizing atomically precise carbon nanostructures, particularly graphene nanoribbons (NRs), employing advanced synthetic methodologies. Despite these advancements, achieving control over the stereochemistry of twisted NRs has proven to be a formidable challenge. This manuscript presents a strategic approach to achieve absolute control over the single-handed helical conformation in a cove-edged NR. This strategy leverages enantiopure helicenes as a molecular wrench, intricately influencing the overall conformation of the NR. [7]helicenes stitched to the terminal K-regions of a conjugated pyrene NR through a stereospecific annulative  $\pi$ -extension reaction to produce a helically twisted NR with an end-to-end twist of 171°. Furthermore, a detailed investigation of the impact of twisting on the conformational population was studied by quantum chemical calculations.

Received 18th March 2024

Accepted 15th May 2024

DOI: 10.1039/d4sc01814a

rsc.li/chemical-science

## Introduction

The electronic properties of graphene nanoribbons (NRs)<sup>1–8</sup> composed of linearly fused polycyclic aromatic hydrocarbons (PAHs) depend on their size, shape, and most importantly, edge structures. Based on the edges NRs can be classified as cove-edge, armchair-edge, and zigzag-edge NRs.<sup>9–13</sup> The cove-edge NRs<sup>14</sup> are of special interest as they have the potential to be chiral as a result of the non-planarity arising from the steric hindrance in the cove regions. Cove-edged NRs can adopt a twisted configuration, whether helical or wagging (randomly twisted), contingent upon specific steric congestion along their edges.<sup>15–18</sup> However, they suffer from low configurational stability and the minimal relative energy difference between helical and wagging conformers due to the rapid flipping of the inner cove's chirality.<sup>14,19,20</sup> The NRs with *fold* regions—such as supertwistacene<sup>21</sup> by Wang *et al.* and triply conjugated HBC (hexa-*peri*-hexabenzocoronene)<sup>22</sup> by Campana *et al.*—exhibit a slightly higher barrier, allowing room temperature chiral resolution. The nanographenes with bay regions are relatively difficult to twist, as the majority of the rings lie flat in the orthogonal plane with limited options for substitution.

Chalifoux *et al.* achieved a 35° end-to-end twist by substituting only one side of the bay region,<sup>23</sup> while Würthner *et al.* substituted all positions in the bay region, resulting in an enhanced twist of 76° in quaterylene bisimide with an enantiomerization barrier of 30 kcal mol<sup>−1</sup>.<sup>24</sup>

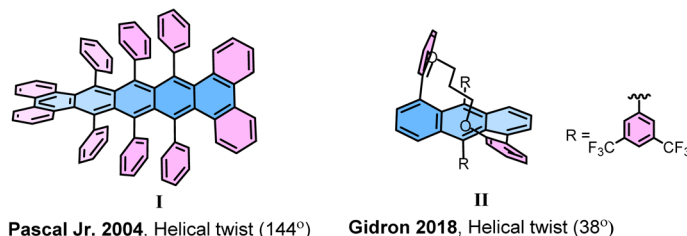
The strategy of strain-induced twist has been widely applied to achieve longitudinally twisted acenes ('twistacenes'), the narrowest NRs, which can be manipulated into helical or wagging conformations through the strategic application of crowded substitutions or benzyl annulations (Fig. 1).<sup>4,25–27</sup> In the late 1990s, Pascal Jr *et al.* pioneered the twisting of acenes by employing bulky phenyl substitutions reaching an astonishing end-to-end twist of 144° (**I**).<sup>28–30</sup> This record was surpassed by Kilway *et al.* in 2018 with the hexacene derivative, achieving an end-to-end twist of 184°. In twistacenes, the strain-induced helical twist propagates along the aromatic ring planes. However, often twistacenes owing to the low configurational stability cannot be resolved into enantiomers. Gidron *et al.* engineered helically locked tethered anthracenes (**II**), which can be isolated in an enantiopure form, achieving an end-to-end twist of up to 38°. Several attempts were made to incorporate promising  $\pi$ -electron-rich cores, such as pyrenes<sup>34</sup> into twisted acenes. In most cases, the attachment takes place at the K-region of the pyrene, as it offers greater accessibilities compared to other reaction sites of pyrene. Wudl and Zhang developed a molecule (**III**) containing a pentacene core terminally locked by two pyrenes.<sup>35</sup> However, it failed to propagate a uniform twist from one end to the other as the twist reverses at the central benzene ring due to the absence of steric groups at crucial positions in the central acene. King *et al.* prepared a K-

<sup>a</sup>Julius-Maximilians-Universität Würzburg, Institut für Organische Chemie, Am Hubland, 97074 Würzburg, Germany. E-mail: princekumar.ravat@uni-wuerzburg.de

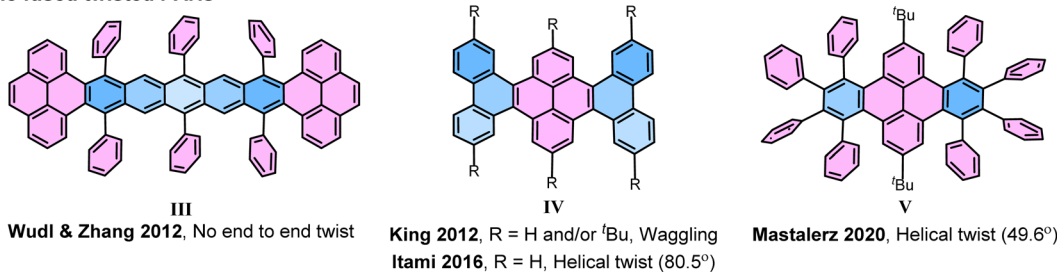
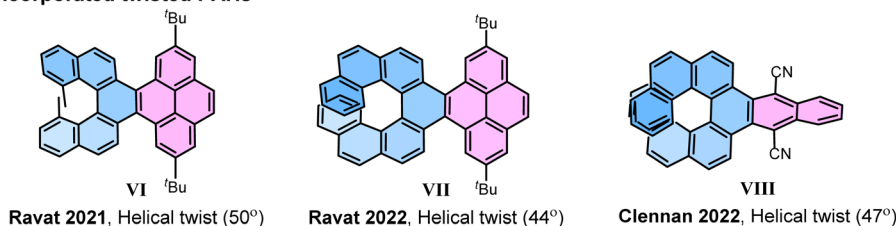
<sup>b</sup>Julius-Maximilians-Universität Würzburg, Institut für Anorganische Chemie, Am Hubland, 97074 Würzburg, Germany

† Electronic supplementary information (ESI) available. CCDC 2315652 and 2315653. For ESI and crystallographic data in CIF or other electronic format see DOI: <https://doi.org/10.1039/d4sc01814a>

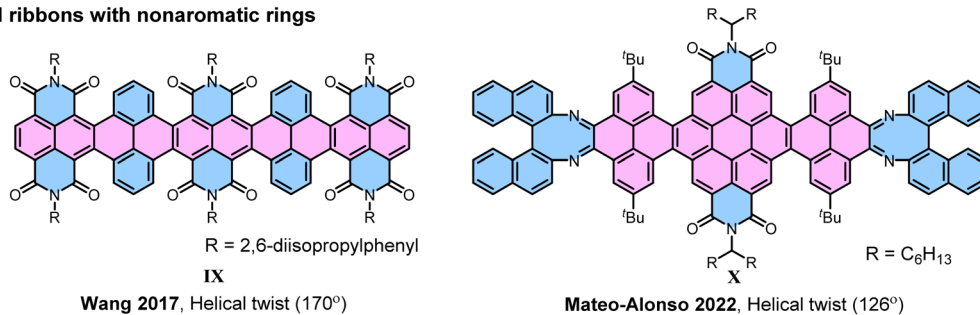
## (a) Strain induced twistacene



## (b) Pyrene fused twisted PAHs

(c)  $[n]$ Helicene incorporated twisted PAHs

## (d) Twisted ribbons with nonaromatic rings



## (e) This work: Stereoselective strain induced helical twist

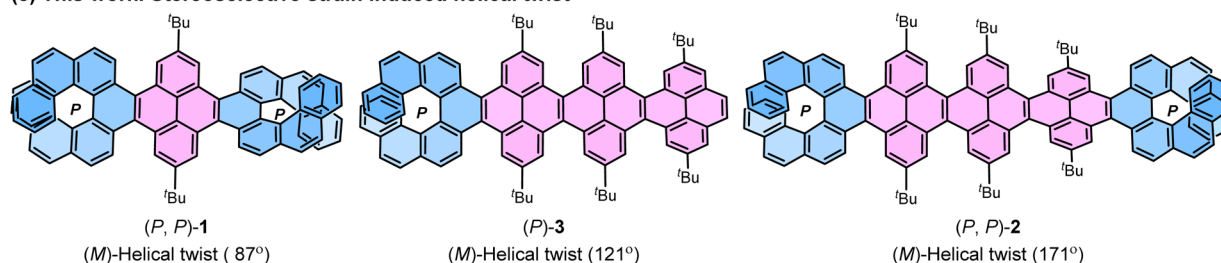


Fig. 1 Selected previous examples of twisted molecules (a)–(d) and newly synthesized helically twisted NRs (e). The helical end-to-end twist is reported in parenthesis.

region phenanthrene annulated pyrene exhibiting wagging conformation (**IV**).<sup>36</sup> In contrast, later Itami *et al.* achieved the helical conformation of **IV** with an unsubstituted core.<sup>37</sup> Lately, eight phenyl substituted dibenzo[*e*, *l*]pyrene (**V**) by Mastalerz *et al.* showed the helical structure with an end-to-end twist of  $49.6^\circ$ .<sup>38</sup> Recently, we introduced  $[n]$ helicene as a strain-inducing tensor for generating twisted acene core within a pyrene-fused  $[n]$ helicene moiety, achieving end-to-end twist of  $50^\circ$  by

incorporating methyl substituted  $[5]$ helicene at the K-region of pyrene (**VI**) and a  $44^\circ$  end-to-end twist upon using  $[7]$ helicene (**VII**).<sup>39–41</sup> The helicity of twisted core was dictated by the helicity of the attached  $[n]$ helicene, which was opposite to each other. This approach was then followed by Clennan to produce a  $47^\circ$  end-to-end twist in a  $[7]$ helicene-incorporated anthracene (**VIII**).<sup>42</sup> Mateo-Alonso *et al.* consequently employed this concept in making a pyrene-coronene cored helical nanoribbon (**X**),



where enantiopure 1,1'-binaphthyl-2,2'-diamine was fused to form [5]helicenoid at both terminal ends containing distorted octagonal rings with four cove region [4]helicene subunits achieving an end-to-end twist of 126° for the central core.<sup>43</sup> It is worth mentioning that, similar to **X**, Wang *et al.* in 2017 reported a helically twisted decatwistacene (**IX**) with a much higher end-to-end torsion twist of 170° which was achieved solely through steric hindrance between imide groups and benzene rings in the cove region, without the use of any external steric tensor such as [n]helicinoids, as shown in **X**.<sup>44</sup> The axially chiral binaphthyl moiety within the ribbon **X** is not fully conjugated and possesses multiple nonaromatic rings with two nitrogen atoms, as well as two imide moieties. Furthermore, in this ribbon, the cove-region gained additional configurational stability from the buttressing effect<sup>45</sup> of imide moieties. The conformation of **X** was susceptible to temperature fluctuations because of the dynamic nature of the cove regions. Hence, the challenge of developing a sturdy cove-edged hydrocarbon nanoribbon with a precisely stable conformation remains unaddressed.

Earlier investigations into strain-induced twisting suffered from limitations in controlling stereochemistry and low configurational stability, making it a challenging endeavor to synthesize helically twisted chiral hydrocarbon NRs in a stereospecific manner. To address this challenge, we aimed to exert precise control over the twist of cove-edged NRs by integrating configurationally stable enantiopure [n]helicenes<sup>46–49</sup> at the terminals preceding our earlier work where we attain 99.5% conformational stability for **VII**. The incorporation of enantiopure [n]helicene on both ends of NRs gives rise to three potential stereoisomers: left-handed, right-handed, or wagging. In this study, we demonstrate that the overall conformation and twist of cove-edged NRs can be systematically adjusted by employing terminal helicene moieties, effectively acting as a molecular wrench. This article presents a strategic methodology focused on achieving helically twisted chiral nanoribbons, featuring a central pyrene core NR, securely anchored at terminal K-regions through one or two [7]helicenes *via* stereospecific APEX reactions (Fig. 1e). The influence of [7]helicene on stabilizing the conformers was explored using DFT-optimized structures and single-crystal structure analysis. The (chir)optical properties were comprehensively examined through UV-Vis absorption, emission, electronic circular dichroism (ECD), and circularly polarized luminescence (CPL) spectroscopies. Furthermore, the inversion barrier of compound **1** was estimated through kinetic measurements. The experimental findings were effectively correlated with quantum chemical calculations, providing a comprehensive understanding of the synthesized helically twisted chiral nanoribbons and their intriguing properties.

## Results and discussion

### Synthesis and characterization

The most straightforward instance of cove-edged nanoribbons (NRs) involves a linearly fused pyrene connected at the K-region. In this study, a central NR comprising three linearly fused pyrene units (**3Py**) was selected. The *peri*-fused benzene rings in

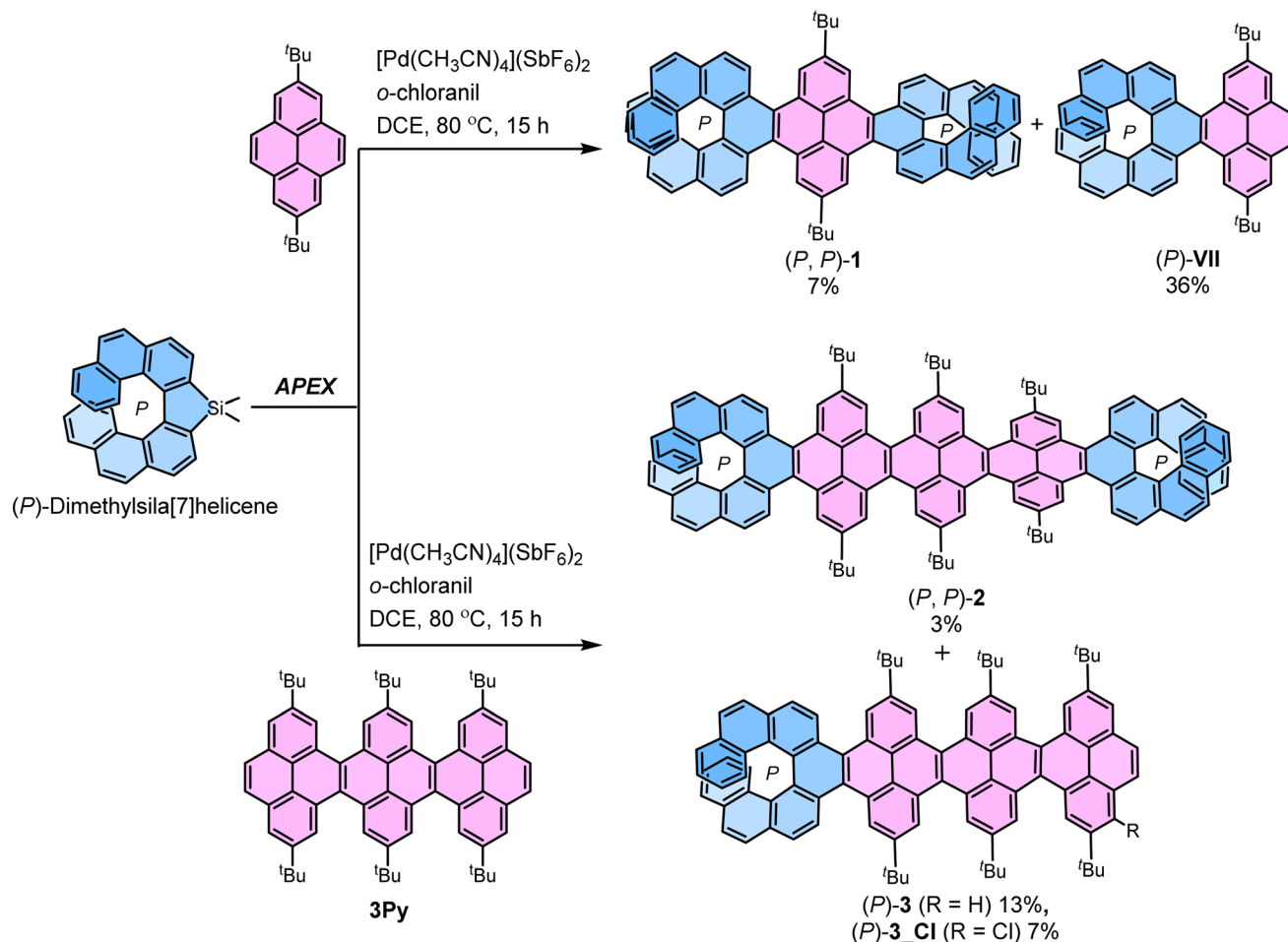
pyrene served to anchor essential points necessary for transmitting twists from one end to the other. Recently, we developed a stereospecific method for incorporating [n]helicene at the K-region of pyrene through a one-pot Suzuki coupling – C–H activation process.<sup>39–41</sup> Initially, we applied the same strategy to synthesize (*P, P*)-**1** by conducting a one-pot Suzuki coupling – C–H activation reaction between (*S*)-3,3-dibromo-4,4'-biphenanthrene<sup>40</sup> (*ee* > 99%) and 2-(2,7-di-*tert*-butylpyren-4-yl)-4,4,5,5-tetramethyl-1,3,2-dioxaborolane.<sup>50</sup> (*P, P*)-**1** was successfully obtained with a moderate 35% yield, considering two Suzuki coupling and two C–H activation reaction steps (ESI Section S2†). However, this approach proved unsuitable for synthesizing **2** and **3** due to inaccessibility of required pyrene-NR (**3Py**) with boronic ester group. To surmount these obstacles, we adopted the K-region specific annulative  $\pi$ -extension (APEX) reaction developed by Ito and Itami (Scheme 1).<sup>51</sup>

(*P, P*)-**1** and (*P, P*)-**2** were synthesized from 2,7-di-*tert*-butylpyrene and **3Py**,<sup>52</sup> and (*P*)-dimethylsila[7]helicene (*ee* > 99%),<sup>53</sup> through a palladium-catalyzed double C–H/C–Si coupling (K-region APEX reaction).<sup>51</sup> A mixture of the respective pyrene precursor and (*P*)-dimethylsila[7]helicene was heated at 80 °C for 15 hours in the presence of [Pd(CH<sub>3</sub>CN)<sub>4</sub>](SbF<sub>6</sub>)<sub>2</sub> and *o*-chloranil, producing the double annulative (*P, P*)-**1** and (*P, P*)-**2** with stereospecificity. The second competitive addition of [7]helicene occurs selectively at the K-region of the pyrene possibly due to its high olefinic character,<sup>54</sup> compared to the two K-regions of the first annulated [7]helicene where aromatic character is dominant.<sup>51</sup> This selectivity can be rationalized by the presence of neighboring conjugated Clar's sextet. In the K-region of pyrene, four *peri*-fused benzene rings shared two Clar's sextets, whereas in the K-region of [7]helicene, it conjugates with two neighboring Clar's sextets. The APEX reactions also produced single annulated (*P*)-**3** and (*P*)-**VII** (ref. 40) with moderate yield. Similarly, (*M, M*)-**1** and (*M, M*)-**2** were synthesized from (*M*)-dimethylsila[7]helicene in comparable yields and enantiopurity. The identical enantiopurity of **1** (*ee* > 99%) in APEX reaction and Suzuki coupling–C–H activation confirms the stereospecificity of the APEX reaction (ESI Fig. S1†). To the best of our knowledge, these are the first examples of site-selective and stereospecific APEX reactions, as the enantiomeric excess (*ee*) was retained throughout the reaction scheme.<sup>55</sup> The structures of **1**, **2** and **3** were confirmed by unambiguous assignment of <sup>1</sup>H and <sup>13</sup>C peaks to the respective atoms by COSY, NOESY, HSQC, and HMBC NMR measurements (ESI Fig. S10†). Additionally, the structure of **1** and **3Py** was determined by single-crystal X-ray diffraction (ESI Fig. S9†).

### Pyrene bridged double [7]helicene

Before exploring longer fused pyrene NRs, an extensive study was conducted on conformational stability of pyrene bridged double [7]helicene (**1**). DFT optimized geometry and energy level analyses of (*P, P*)-**1** revealed that the diastereomer with an opposite chirality in the cove region to [7]helicene (left-handed helical conformation) is notably most stable, constituting a relative Boltzmann population of 99.9% (Fig. 2a). The remaining 0.1% encompasses the higher energy wagging conformation of (*P, P*)-





Scheme 1 Synthesis of *(P, P)*-1, *(P, P)*-2 and *(P)*-3 via stereospecific APEX reaction.

1. The theoretical calculations were substantiated by the obtained single crystal structure of *(P, P)*-1 (Fig. 2c), where all four [4]helicene subunits adopt the *M* conformation. The resemblance between the experimental (87°) and calculated (96°) end-to-end twists confirm the precision of the DFT optimized structures. In the case of *(P, M)*-1, pyrene bridged by two [7]helicenes with opposite chirality, the scenario reverses, just the opposite of *(P, P)*-1. The wagging conformation with opposite helicity to [7]helicene in the cove is the most stable, representing 99% of the relative population (Fig. 2b). The remaining 1% comprises the helical conformation. Notably, in both *(P, P)*-1 and *(P, M)*-1, the conformer with similar helicity in the cove and adjacent [7]helicene represents the highest energy conformation, with an almost negligible relative population.

The 99.9% conformational stability of *(P, P)*-1 allow us to assess the configurational stability, unlike the dynamic nanoribbon (**VII**) reported by Mateo-Alonso *et al.* where mixture of conformations exists at variable temperature for fixed helicity of the [5]helicenoid.<sup>43</sup> *(P, P)*-1 was heated at elevated temperature to observe formation of other isomers. Upon heating two new peaks appeared in HPLC, which were assigned to *(M, M)*-1 and *(P, M)*-1 (ESI Fig. S2a†). Using Eyring equation the  $\Delta H$  and  $\Delta S$  values were calculated to be 44.1 kcal mol<sup>-1</sup> and 21.4 cal K<sup>-1</sup> mol<sup>-1</sup>, respectively (ESI Fig. S3b†). Accordingly, the Gibbs activation energy  $\Delta G^\ddagger$

(298 K) for diastereomerization of **1** was calculated to be 37.7 kcal mol<sup>-1</sup>, lower than the enantiomerization barrier of pristine [7]helicene (41.2 kcal mol<sup>-1</sup>).<sup>49,56,57</sup> It should be noted that, both  $\Delta H$  and  $\Delta S$  for the diastereomerization of **1** are significantly higher than those for the enantiomerization of the [7]helicene ( $\Delta H = 40.4$  kcal mol<sup>-1</sup>,  $\Delta S = -2.8$  cal K<sup>-1</sup> mol<sup>-1</sup>).<sup>49</sup> Hence the decreased  $\Delta G^\ddagger$  for **1** can be rationalized for the much higher and positive  $\Delta S$  value—an entropically favored process.  $\Delta G^\ddagger$  (438 K) of **1** (35.3 kcal mol<sup>-1</sup>) is slightly higher than that of **VII** (34.1 kcal mol<sup>-1</sup>)<sup>40</sup> indicating a more ordered conformation upon locking the structure with the second [7]helicene.<sup>58</sup> Upon prolonged heating *(P, P)*-1 reaches to a diastereomeric equilibrium of *(P\*, P\*)*-1 to meso *(P, M)*-1 at a ratio of 3.6 : 1 (ESI Fig. S1 and S2†), similar to the ratio (3.8 : 1) obtained from racemic reaction (ESI Fig. S1†). This is well in accordance with the calculated relative population of two diastereomers (3.8 : 1) by DFT.

### Conformation isomers of conjugated cove-edged NR (3Py)

The cove-edged nanoribbons showcase a nonplanar geometry primarily attributed to steric repulsion between two hydrogen atoms positioned at the inner core of recurring [4]helicene units, resulting in tilted upward and downward topologies. The conformational stability of **3Py** was evaluated through DFT



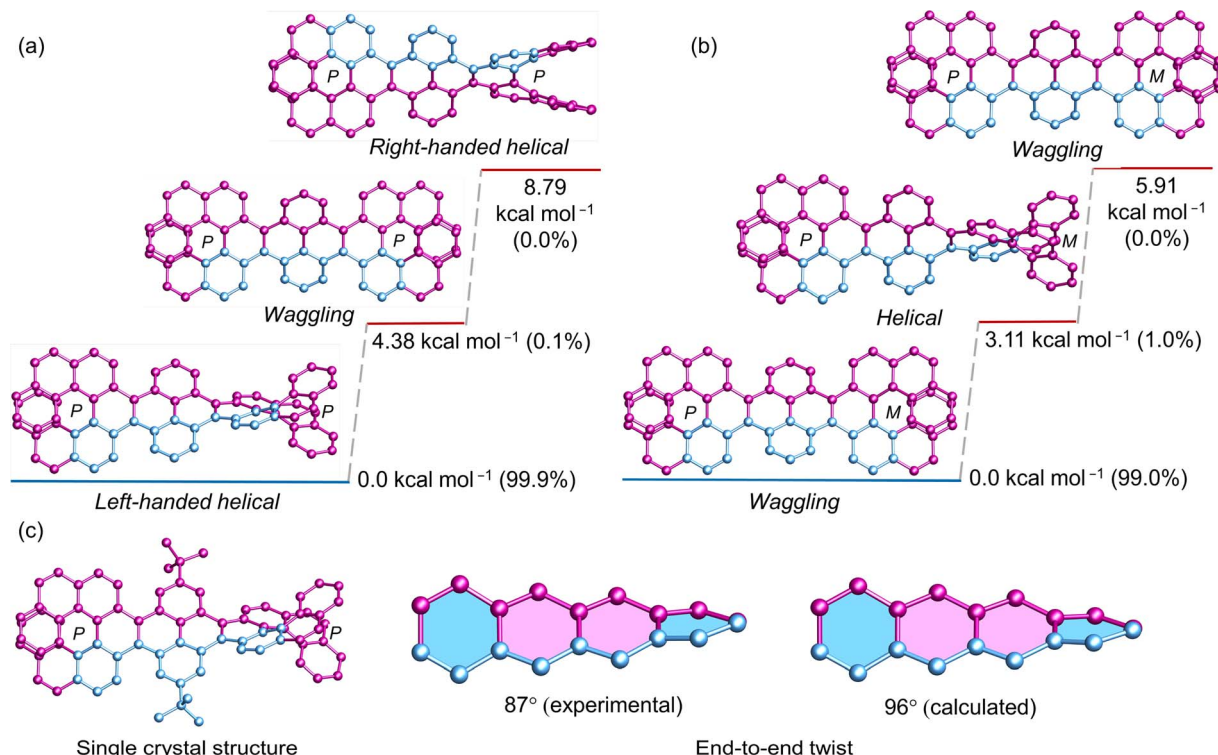


Fig. 2 DFT ( $\omega$ B97XD/6-31G(d,p)) calculated conformational isomers of (a) (*P, P*)-1, (b) (*P, M*)-1 with relative total energy and population at 298 K. (c) Single crystal structure of (*P, P*)-1. Hydrogen atoms in all and *tert*-butyl groups in calculated structures are omitted for clarity.

calculations (Fig. 3). At room temperature, the wagging conformer of **3Py** prevails as the most stable, constituting 78% of the population, while the remaining portion corresponds to the helical conformer. The calculations were substantiated by the obtained single crystal of **3Py**, revealing a wagging twist. Notably, there is no net end-to-end twist observed, as the twist from one terminal to the other end does not continue consistently but instead reverses the twist direction in the middle pyrene. The rapid flipping of adjacent pyrene in wagging twist is evident from the  $^1\text{H}$  NMR experiment, where all *tert*-butyl groups exhibit only one distinct sharp singlet at 1.63 ppm (ESI Fig. S15 $^\dagger$ ).

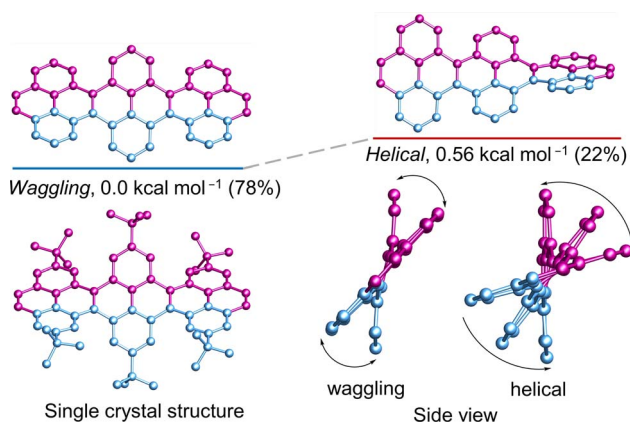


Fig. 3 DFT ( $\omega$ B97XD/6-31G(d,p)) calculated conformational isomers and single crystal structure of **3Py** with relative total energy and population at 298 K. Hydrogen atoms in all and *tert*-butyl groups in calculated structures are omitted for clarity.

### Effect of one terminal [7]helicene on conformational stability of cove-edged NR

Next, we investigated the influence of one (*P*)-[7]helicene unit on the conformation of **3Py**. Although (*P*)-**3** appears as flexible as **3Py**, the left-handed helical conformation emerges as the most stable, constituting a relative population of 87.9% (Fig. 4). Conversely, the lowest wagging conformer, slightly higher in energy (1.91 kcal mol $^{-1}$ ), accounts for a relative population of 6.3%, while combined population of all four wagging conformers amounts to 12.09%. The highest energy right-handed helical conformer (5.17 kcal mol $^{-1}$ ) comprises only 0.01% of the population. Despite numerous attempts in various solvent combinations and at low temperatures, obtaining a single crystal of (*P*)-**3** remained elusive. However, the twisted structure of the  $C_2$  symmetric (*P*)-**3** is discernible in the  $^1\text{H}$  NMR, where all three sets of *tert*-butyl groups exhibit three distinct singlet signals, each corresponding to 18 protons (ESI Fig. S32 $^\dagger$ ). Consequently, rapid flipping of adjacent pyrenes in the wagging conformation just as **3Py** is not applicable to (*P*)-**3**. The end-to-end twist of (*P*)-**3** measures 121 $^\circ$ , which is 34 $^\circ$  higher than that of (*P, P*)-**1**.

### Effect of two terminal [7]helicenes on conformational stability of cove-edged NR

The (*P*)-[7]helicene-locked nanoribbon (*P, P*)-**2** follows a similar trend as (*P*)-**3** and (*P, P*)-**1** established by DFT calculated energies. The left-handed helical nanoribbon represents the most stable conformer with a relative population of 99.9%, while the





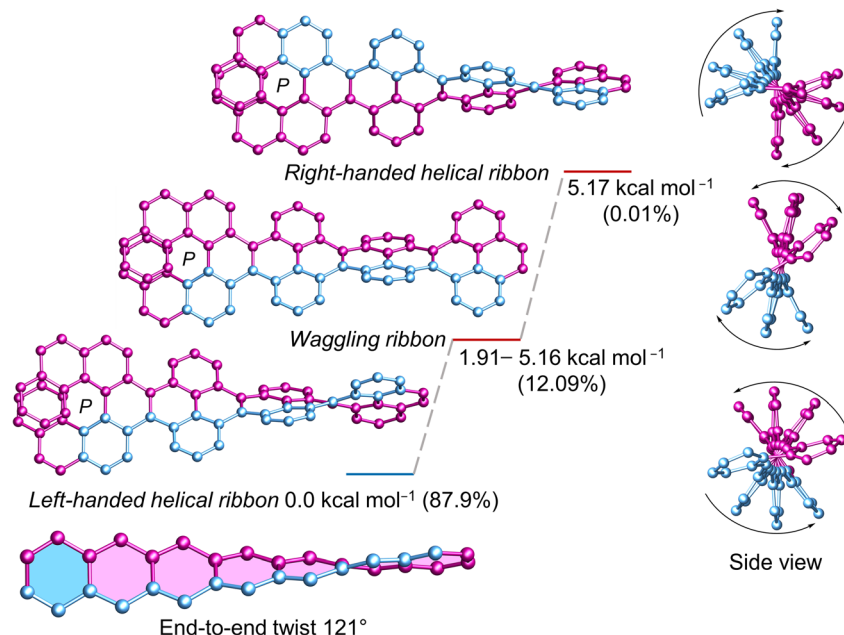


Fig. 4 DFT ( $\omega$ B97XD/6-31G(d,p)) calculated conformational isomers of (*P*)-3 with relative total energy and population at 298 K. The lowest energy wagging conformation of (*P*)-3 is depicted here. Refer to ESI Section S6† for additional wagging conformations. Hydrogen atoms and *tert*-butyl groups are omitted for clarity.

wagging conformers account for the remainder (Fig. 5a). The right-handed helical ribbon represents the highest energy conformer ( $9.22 \text{ kcal mol}^{-1}$ ) with a negligible population. Notably, upon locking both terminal K-regions by (*P*)-[7]helicene in 2,7-di-*tert*-butyl pyrene and **3Py**, the left-handed helical ribbon becomes stabilized by  $4.37\text{--}4.38 \text{ kcal mol}^{-1}$  from the lowest wagging conformer and by  $8.79\text{--}9.22 \text{ kcal mol}^{-1}$  from the right-handed helical ribbon. In the case of (*P*, *M*)-2, where helicenes of opposite chirality attached to the terminal of NR, the wagging conformer is stable by  $2.57 \text{ kcal mol}^{-1}$  from the helical conformer, constituting a relative population of 65% (Fig. 5b). Although (*P*, *P*)-2 possesses twice the number of labile [4]helicene subunits in comparison to the pyrene-coronene nanoribbon (**X**) described by Mateo-Alonso *et al.*,<sup>43</sup> its left-handed helical conformer shows significantly greater stability than the wagging conformers, comprising a relative population of 99.9% *versus* 93.8%. The end-to-end twist of (*P*, *P*)-2 measures  $171^\circ$  making it as the second-most twisted central acene core following the twisted hexacene reported by Kilway *et al.*<sup>31</sup> The end-to-end twist in (*P*, *P*)-2 is nearly double that of (*P*, *P*)-1 and increased significantly from (*P*)-3 demonstrating that the terminal [7]helicenes act as a molecular wrench in maintaining the twist. The average torsion angle per benzene ring<sup>4</sup> measures  $21.75^\circ$  and  $21.38^\circ$  in (*P*, *P*)-1 and (*P*, *P*)-2, respectively, in contrast to  $17.3^\circ$  in (*P*)-3 and  $14.8^\circ$  in (*P*)-VII, which highlights the increased strain resulting from the conformational lock imposed by the second [7]helicene. The distance between the terminal benzene centroids of [7]helicene substructure decreased significantly from  $4.13 \text{ \AA}$  in (*P*, *P*)-1 to  $3.77 \text{ \AA}$  in (*P*, *P*)-2, while the torsional twist slightly increased from  $22.4^\circ$  (**1**) to  $22.9^\circ$  in **2**. This highlights the additional strain imposed by the [7]helicene in (*P*, *P*)-2 to maintain such a high level of twist in

the central core. Regardless of its size ( $\sim 3.1 \text{ nm}$ ), and the extensive aromatic core comprising 100 carbon atoms, (*P*, *P*)-2 demonstrates excellent solubility in a wide range of organic solvents, owing to the highly twisted structure.

### Nucleus-independent chemical shift calculations

To evaluate the effect of twisting on the aromaticity, the nucleus-independent chemical shift (NICS) values were computed for all discussed molecules (Fig. 6). All benzene rings exhibited negative NICS(1)<sub>zz</sub> values, indicative of their aromaticity, except for H4 ring in (*P*)-3 and (*P*, *P*)-2. The marginally positive value NICS(1)<sub>zz</sub> for ring H4 in (*P*)-3 and (*P*, *P*)-2 corroborates to its highly distorted structure compared to other rings. In the [7]helicene subunit of NRs, the aromaticity increased on moving away from the central rings (H4 to H1) similar to pristine [7]helicene.<sup>59,60</sup> Aromaticity within the acene core (P1 to P6) decreases on moving away from terminal rings into the central core in **3Py**. However, this trend reverses in (*P*, *P*)-1 and (*P*, *P*)-2 as terminal rings (P1 or P6) show smaller NICS(1)<sub>zz</sub> values with a gradual increase to the inner core. Away from the centrally tethered twisting, the P7–P9 rings in the pyrene exhibit relatively higher negative NICS(1)<sub>zz</sub> values, as do the H1 and H2 rings of the [7]helicene. In general, the NICS(1)<sub>zz</sub> values of the wagging conformer of **1** and **2** are significantly higher than those of the left-handed helical conformer of (*P*, *P*)-1 and (*P*, *P*)-2, likely due to absence of an end-to-end twist (ESI Table S6†).

### Chiroptical properties

The absorption and emission spectra of (*P*, *P*)-2 and (*P*)-3 closely resemble each other, with a slight red shift compared to (*P*, *P*)-1, due to an increase in  $\pi$ -conjugation (Fig. 7a). The optical energy



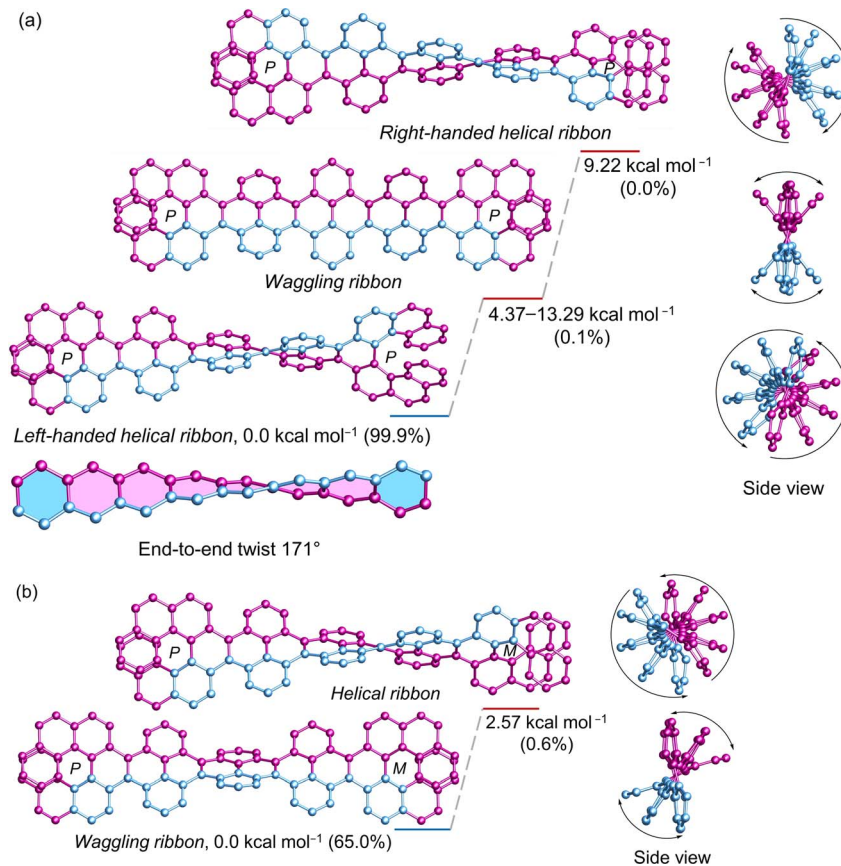


Fig. 5 DFT ( $\omega$ B97XD/6-31G(d,p)) calculated conformational isomers of (a) (P, P)-2 and (b) (P, M)-2 with relative total energy and population at 298 K. The lowest energy wagging conformation of 2 is depicted here. Refer to ESI Section S6† for additional wagging conformations. Hydrogen atoms and *tert*-butyl groups are omitted for clarity.

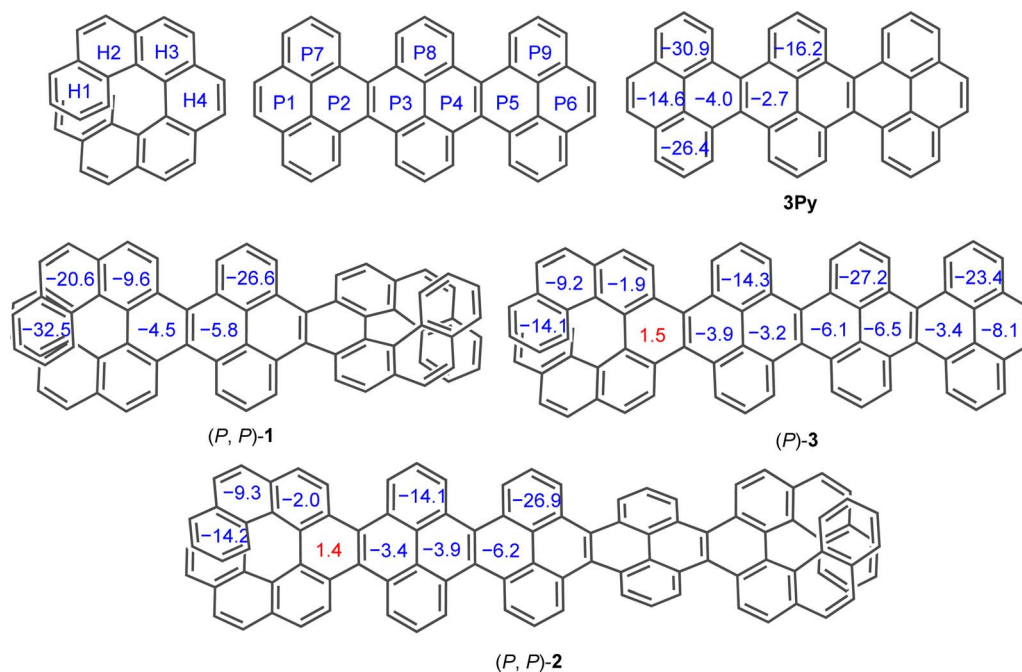


Fig. 6 Calculated (GIAO-B3LYP/6-311+G(2d,p)) NICS(1)<sub>zz</sub> values for 3Py, (P, P)-1, (P, P)-2 and (P)-3. *tert*-Butyl groups are omitted for clarity.





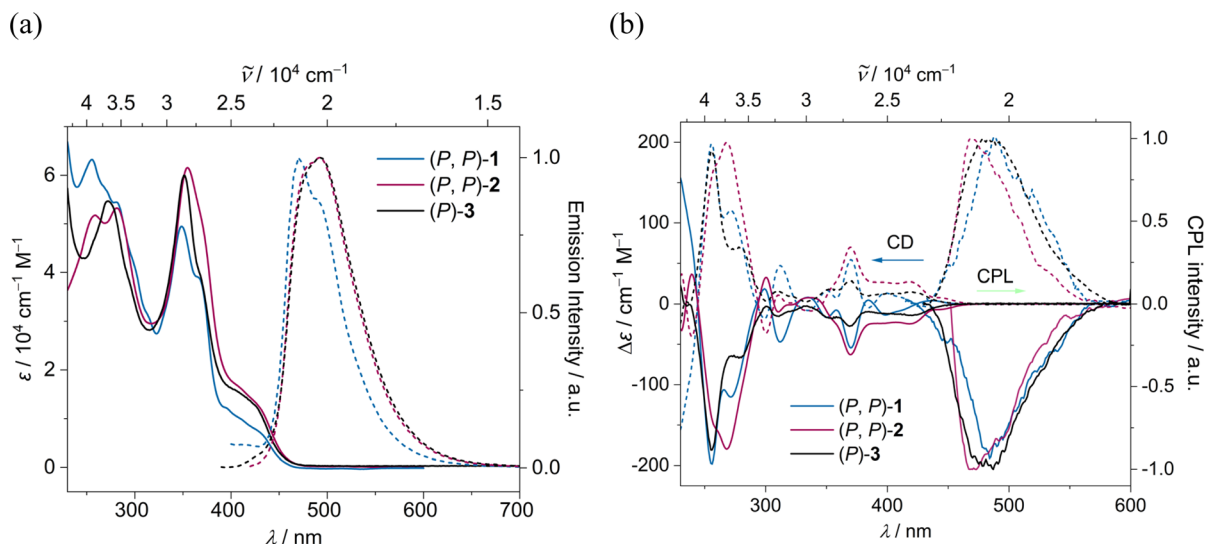


Fig. 7 (a) UV-Vis absorption (solid line) and emission (dashed line) spectra and (b) ECD and CPL spectra of (*P, P*) (solid line) and (*M, M*) (dashed line) of 1 (blue), 2 (red) and 3 (black) in DCM ( $c \sim 10^{-5} \text{ M}$ ).

gap for (*P, P*)-1, (*P, P*)-2, and (*P*)-3 falls within the range of 2.79–2.83 eV, notably lower than that of [7]helicene (3.06 eV)<sup>61</sup> and 3Py (2.92 eV) (ESI Table S2†). TD-DFT (B3LYP/6-31g(d,p)) calculations revealed that for all three compounds the lowest energy absorption band mainly stemming from HOMO  $\rightarrow$  LUMO transition with similar oscillator strength of 0.13–0.14 (ESI Table S5†). The emission maximum for (*P, P*)-1, (*P, P*)-2 and (*P*)-3 were recorded at 473, 492 and 493 nm respectively with fluorescence quantum yields (FQYs) of 0.05, 0.15 and 0.19 in dichloromethane. The decrease in FQY of (*P, P*)-2 compared to (*P*)-3 can be attributed to twist-enhanced inter system crossing as observed in twisted acenes.<sup>62,63</sup> The fluorescence decay lifetimes of (*P, P*)-1, (*P, P*)-2, and (*P*)-3 range between 5.07–5.55 ns, significantly shorter than that of [7]helicene (13.8 ns).<sup>64</sup>

The absolute configuration of the enantiomers of 1, 2, and 3 was assigned comparing experimental and TD-DFT calculated CD spectra (ESI Fig. S8†). The lowest energy CD signals are stronger for 2, followed by 1 and 3 respectively (Fig. 7b). The experimentally obtained luminescence dissymmetry factor ( $g_{\text{lum}}$ ) of 2 is  $1.54 \times 10^{-3}$ , nearly three times that of 3 ( $0.63 \times 10^{-3}$ ) and 1 ( $0.54 \times 10^{-3}$ ) (ESI Fig. S7†). The increase in chiroptical response of 2 can be attributed to the increased twist in the NR core, resulting in macro chirality. This was further supported by TD-DFT calculations, which showed enhanced excited state magnetic transition dipole moment and higher  $\cos \theta$  values for 2 compared to those for 1 and 3 (ESI Table S3†). In contrast to dynamic pyrene-coronene NR (X) reported by Mateo-Alonso *et al.*,<sup>43</sup> the variable temperature (278–333 K) ECD and CPL measurements showed minimal change (ESI Fig. S6f†), indicating the robust chirality of the (*P, P*)-2, corroborating its higher  $g_{\text{lum}}/g_{\text{abs}}$  ratio of 0.81.<sup>65</sup>

## Conclusion

In summary, we have succeeded in achieving unparalleled control over the conformation of cove-edged graphene NRs.

Leveraging enantiopure [7]helicenes as molecular wrenches, we have integrated these helical motifs into the terminal K-regions of a conjugated pyrene NR through a stereospecific APEX reaction. Among these acene-cored NRs, (*P, P*)-2 displayed an impressive end-to-end twist of  $171^\circ$ . These robust chiral NRs exhibited exceptional configurational and conformational stability with a relative population of helical NR amounting to 99.9% at room temperature. The progressive increase in chiroptical responses from (*P*)-3 to (*P, P*)-2 highlights the emergence of macro chirality resulting from the overall twist of the nanoribbon. Our study not only addresses the longstanding challenge of controlling the stereochemistry of twisted hydrocarbon NRs but also sheds light on the impact of twisting on the conformational population. Through extensive quantum chemical calculations, we have provided a detailed understanding of the energetically favored conformers and their relative populations. The outlined strategy, allowing the late-stage introduction of helicene units by APEX reaction, holds promise for facilitating the synthesis of diverse cove edge NR variants with desired conformations.

## Data availability

The experimental procedures, characterizations, spectral analysis and DFT computational details are available in the ESI.†

## Author contributions

A. S. performed the experimental work, analyzed the data, and wrote the manuscript. K. R. and H. B. analyzed the crystallographic data. P. R. conceived the project, supervised the research, and prepared the final draft of the manuscript.

## Conflicts of interest

There are no conflicts to declare.



## Acknowledgements

We dedicate this paper to Professor Frank Würthner (University of Würzburg) on the occasion of his 60th birthday. P. R. thanks Julius-Maximilians-Universität Würzburg for “Excellent Ideas” program. A. S. and P. R. sincerely thank Prof. Christoph Lambert (University of Würzburg) for generously supporting our research. Funding: this project received funding from Deutsche Forschungsgemeinschaft (DFG) (Project No. 448604676). The CPL/CD hybrid spectrometer was funded by the DFG (Project No. 444286426). We thank the reviewers for their valuable suggestions to improve the manuscript.

## References

- 1 X.-Y. Wang, A. Narita and K. Müllen, Precision synthesis versus bulk-scale fabrication of graphenes, *Nat. Rev. Chem.*, 2017, **2**, 0100.
- 2 J. M. Fernández-García, P. J. Evans, S. Filippone, M. Á. Herranz and N. Martín, Chiral Molecular Carbon Nanostructures, *Acc. Chem. Res.*, 2019, **52**, 1565–1574.
- 3 Y. Segawa, H. Ito and K. Itami, Structurally uniform and atomically precise carbon nanostructures, *Nat. Rev. Mater.*, 2016, **1**, 15002.
- 4 M. Rickhaus, M. Mayor and M. Jurićek, Strain-induced helical chirality in polyaromatic systems, *Chem. Soc. Rev.*, 2016, **45**, 1542–1556.
- 5 J. R. Sanchez-Valencia, T. Dienel, O. Gröning, I. Shorubalko, A. Mueller, M. Jansen, K. Amsharov, P. Ruffieux and R. Fasel, Controlled synthesis of single-chirality carbon nanotubes, *Nature*, 2014, **512**, 61.
- 6 S. Eigler and A. Hirsch, Chemistry with Graphene and Graphene Oxide—Challenges for Synthetic Chemists, *Angew. Chem., Int. Ed.*, 2014, **53**, 7720–7738.
- 7 E. Clar, *Polycyclic Hydrocarbons*, Springer, 1964.
- 8 W. Niu, Y. Fu, Z.-L. Qiu, C. J. Schürmann, S. Obermann, F. Liu, A. A. Popov, H. Komber, J. Ma and X. Feng,  $\pi$ -Extended Helical Multilayer Nanographenes with Layer-Dependent Chiroptical Properties, *J. Am. Chem. Soc.*, 2023, **145**, 26824–26832.
- 9 A. Narita, X. Feng and K. Müllen, Bottom-Up Synthesis of Chemically Precise Graphene Nanoribbons, *Chem. Rev.*, 2015, **15**, 295–309.
- 10 A. Narita, X.-Y. Wang, X. Feng and K. Müllen, New advances in nanographene chemistry, *Chem. Soc. Rev.*, 2015, **44**, 6616–6643.
- 11 S. Dutta and S. K. Pati, Novel properties of graphene nanoribbons: a review, *J. Mat. Chem.*, 2010, **20**, 8207–8223.
- 12 J. Liu, R. Berger, K. Müllen and X. Feng, in *From Polyphenylenes to Nanographenes and Graphene Nanoribbons*, Springer, 2017, vol. 278, pp. 1–32.
- 13 J. Li, S. Sanz, N. Merino-Díez, M. Vilas-Varela, A. Garcia-Lekue, M. Corso, D. G. de Oteyza, T. Frederiksen, D. Peña and J. I. Pascual, Topological phase transition in chiral graphene nanoribbons: from edge bands to end states, *Nat. Commun.*, 2021, **12**, 5538.
- 14 J. Liu, B.-W. Li, Y.-Z. Tan, A. Giannakopoulos, C. Sanchez-Sanchez, D. Beljonne, P. Ruffieux, R. Fasel, X. Feng and K. Müllen, Toward Cove-Edged Low Band Gap Graphene Nanoribbons, *J. Am. Chem. Soc.*, 2015, **137**, 6097–6103.
- 15 Y. Gu, R. Muñoz-Mármol, S. Wu, Y. Han, Y. Ni, M. A. Díaz-García, J. Casado and J. Wu, Cove-Edged Nanographenes with Localized Double Bonds, *Angew. Chem., Int. Ed.*, 2020, **59**, 8113–8117.
- 16 Y. Gu, V. Vega-Mayoral, S. Garcia-Orrit, D. Schollmeyer, A. Narita, J. Cabanillas-González, Z. Qiu and K. Müllen, Cove-Edged Hexa-*peri*-hexabenzobis-*peri*-octacene: Molecular Conformations and Amplified Spontaneous Emission, *Angew. Chem., Int. Ed.*, 2022, **61**, e202201088.
- 17 X. Wang, J. Ma, W. Zheng, S. Osella, N. Arisnabarreta, J. Droste, G. Serra, O. Ivasenko, A. Lucotti, D. Beljonne, M. Bonn, X. Liu, M. R. Hansen, M. Tommasini, S. De Feyter, J. Liu, H. I. Wang and X. Feng, Cove-Edged Graphene Nanoribbons with Incorporation of Periodic Zigzag-Edge Segments, *J. Am. Chem. Soc.*, 2022, **144**, 228–235.
- 18 W. A. Chalifoux, The Synthesis of Non-planar, Helically Coiled Graphene Nanoribbons, *Angew. Chem., Int. Ed.*, 2017, **56**, 8048–8050.
- 19 M. Daigle, D. Miao, A. Lucotti, M. Tommasini and J.-F. Morin, Helically Coiled Graphene Nanoribbons, *Angew. Chem., Int. Ed.*, 2017, **56**, 6213–6217.
- 20 W. Niu, J. Ma, P. Soltani, W. Zheng, F. Liu, A. A. Popov, J. J. Weigand, H. Komber, E. Poliani, C. Casiraghi, J. Droste, M. R. Hansen, S. Osella, D. Beljonne, M. Bonn, H. I. Wang, X. Feng, J. Liu and Y. Mai, A Curved Graphene Nanoribbon with Multi-Edge Structure and High Intrinsic Charge Carrier Mobility, *J. Am. Chem. Soc.*, 2020, **142**, 18293–18298.
- 21 S. Ma, J. Gu, C. Lin, Z. Luo, Y. Zhu and J. Wang, Supertwistacene: A Helical Graphene Nanoribbon, *J. Am. Chem. Soc.*, 2020, **142**, 16887–16893.
- 22 S. Castro-Fernández, C. M. Cruz, I. F. A. Mariz, I. R. Márquez, V. G. Jiménez, L. Palomino-Ruiz, J. M. Cuerva, E. Maçôas and A. G. Campaña, Two-Photon Absorption Enhancement by the Inclusion of a Tropone Ring in Distorted Nanographene Ribbons, *Angew. Chem., Int. Ed.*, 2020, **59**, 7139–7145.
- 23 W. Yang, R. R. Kazemi, N. Karunathilake, V. J. Catalano, M. A. Alpuche-Aviles and W. A. Chalifoux, Expanding the scope of peropyrenes and teropyrenes through a facile InCl<sub>3</sub>-catalyzed multifold alkyne benzannulation, *Org. Chem. Front.*, 2018, **5**, 2288–2295.
- 24 B. Mählemeister, M. Mahl, H. Reichelt, K. Shoyama, M. Stolte and F. Würthner, Helically Twisted Nanoribbons Based on Emissive Near-Infrared Responsive Quaterylene Bisimides, *J. Am. Chem. Soc.*, 2022, **144**, 10507–10514.
- 25 R. A. Pascal, Twisted Acenes, *Chem. Rev.*, 2006, **106**, 4809–4819.
- 26 R. S. Walters, C. M. Kraml, N. Byrne, D. M. Ho, Q. Qin, F. J. Coughlin, S. Bernhard and R. A. Pascal Jr, Configurationally Stable Longitudinally Twisted Polycyclic Aromatic Compounds, *J. Am. Chem. Soc.*, 2008, **130**, 16435–16441.



- 27 I. I. Schuster, L. Craciun, D. M. Ho and R. A. Pascal, Synthesis of a strained, air-sensitive, polycyclic aromatic hydrocarbon by means of a new 1,4-benzadiyne equivalent, *Tetrahedron*, 2002, **58**, 8875–8882.
- 28 J. Lu, D. M. Ho, N. J. Vogelaar, C. M. Kraml and R. A. Pascal, A Pentacene with a 144° Twist, *J. Am. Chem. Soc.*, 2004, **126**, 11168–11169.
- 29 X. Qiao, M. A. Padula, D. M. Ho, N. J. Vogelaar, C. E. Schutt and R. A. Pascal, Octaphenylnaphthalene and Decaphenylanthracene, *J. Am. Chem. Soc.*, 1996, **118**, 741–745.
- 30 Y. Xiao, J. T. Mague, R. H. Schmehl, F. M. Haque and R. A. Pascal Jr, Dodecaphenyltetracene, *Angew. Chem., Int. Ed.*, 2019, **58**, 2831–2833.
- 31 R. G. Clevenger, B. Kumar, E. M. Menuet and K. V. Kilway, Synthesis and Structure of a Longitudinally Twisted Hexacene, *Chem.–Eur. J.*, 2018, **24**, 3113–3116.
- 32 A. Bedi, L. J. W. Shimon and O. Gidron, Helically Locked Tethered Twistacenes, *J. Am. Chem. Soc.*, 2018, **140**, 8086–8090.
- 33 A. Bedi and O. Gidron, The Consequences of Twisting Nanocarbons: Lessons from Tethered Twisted Acenes, *Acc. Chem. Res.*, 2019, **52**, 2482–2490.
- 34 T. M. Figueira-Duarte and K. Müllen, Pyrene-Based Materials for Organic Electronics, *Chem. Rev.*, 2011, **111**, 7260–7314.
- 35 J. Xiao, H. M. Duong, Y. Liu, W. Shi, L. Ji, G. Li, S. Li, X.-W. Liu, J. Ma, F. Wudl and Q. Zhang, Synthesis and Structure Characterization of a Stable Nonatwistacene, *Angew. Chem., Int. Ed.*, 2012, **51**, 6094–6098.
- 36 B. Kumar, C. E. Strasser and B. T. King, *t*-Butyl Biphenylation of *o*-Dibromoarenes: A Route to Soluble Polycyclic Aromatic Hydrocarbons, *J. Org. Chem.*, 2012, **77**, 311–316.
- 37 Y. Yano, H. Ito, Y. Segawa and K. Itami, Helically Twisted Tetracene: Synthesis, Crystal Structure, and Photophysical Properties of Hexabenz[a,c,f,g,j,l,op]tetracene, *Synlett*, 2016, **27**, 2081–2084.
- 38 S. M. Elbert, K. Baumgärtner, J. A. Esteves, L. Weber, F. Rominger and M. Mastalerz, Pyrene-Based Diarynes as Precursors for Twisted Fused Polycyclic Aromatic Hydrocarbons: A Comparison of Two Routes, *Org. Mater.*, 2020, **02**, 358–361.
- 39 A. K. Swain, K. Kolanji, C. Stapper and P. Ravat, C2- and C1-Symmetric Configurationally Stable Pyrene-Fused [5] Helicenes Connected *via* Hexagonal and Heptagonal Rings, *Org. Lett.*, 2021, **23**, 1339–1343.
- 40 A. K. Swain, K. Radacki, H. Braunschweig and P. Ravat, Pyrene-Fused [7]Helicenes Connected *Via* Hexagonal and Heptagonal Rings: Stereospecific Synthesis and Chiroptical Properties, *J. Org. Chem.*, 2022, **87**, 993–1000.
- 41 A. Swain and P. Ravat, Pyrene bridged double[7]helicene embedded with a heptagonal ring, *Org. Chem. Front.*, 2023, **10**, 3714–3725.
- 42 J. A. Weber, E. L. Clennan and N. Arulsamy, A Computational Physical Organic Study of a Torque, Lock, and Propagate Approach and Validation with the Synthesis of Configurationally Stable First-Generation Helically Twisted Acenes, *Eur. J. Org. Chem.*, 2022, e202101533.
- 43 R. K. Dubey, M. Melle-Franco and A. Mateo-Alonso, Inducing Single-Handed Helicity in a Twisted Molecular Nanoribbon, *J. Am. Chem. Soc.*, 2022, **144**, 2765–2774.
- 44 W. Fan, T. Winands, N. L. Doltsinis, Y. Li and Z. Wang, A Decatwistacene with an Overall 170° Torsion, *Angew. Chem., Int. Ed.*, 2017, **56**, 15373–15377.
- 45 W. Theilacker and H. Böhm, Optically Active 2,2'-Dimethylbiphenyl, the Simplest Atropisomeric Hydrocarbon, *Angew. Chem., Int. Ed.*, 1967, **6**, 251.
- 46 R. H. Martin, The Helicenes, *Angew. Chem., Int. Ed.*, 1974, **13**, 649–660.
- 47 Y. Shen and C. F. Chen, Helicenes: synthesis and applications, *Chem. Rev.*, 2012, **112**, 1463–1535.
- 48 M. Gingras, G. Félix and R. Peresutti, One hundred years of helicene chemistry. Part 2: stereoselective syntheses and chiral separations of carbohelicenes, *Chem. Soc. Rev.*, 2013, **42**, 1007–1050.
- 49 P. Ravat, Carbo[n]helicenes Restricted to Enantiomerize: An Insight into the Design Process of Configurationally Stable Functional Chiral PAHs, *Chem.–Eur. J.*, 2021, **27**, 3957–3967.
- 50 L. Ji, I. Krummenacher, A. Friedrich, A. Lorbach, M. Haehnel, K. Edkins, H. Braunschweig and T. B. Marder, Synthesis, Photophysical, and Electrochemical Properties of Pyrenes Substituted with Donors or Acceptors at the 4- or 4,9-Positions, *J. Org. Chem.*, 2018, **83**, 3599–3606.
- 51 K. Ozaki, K. Kawasumi, M. Shibata, H. Ito and K. Itami, One-shot K-region-selective annulative  $\pi$ -extension for nanographene synthesis and functionalization, *Nat. Commun.*, 2015, **6**, 6251.
- 52 F. Liu, X. Shen, Y. Wu, L. Bai, H. Zhao and X. Ba, Synthesis of ladder-type graphene ribbon oligomers from pyrene units, *Tetrahedron Lett.*, 2016, **57**, 4157–4161.
- 53 H. Oyama, K. Nakano, T. Harada, R. Kuroda, M. Naito, K. Nobusawa and K. Nozaki, Facile Synthetic Route to Highly Luminescent Sila[7]helicene, *Org. Lett.*, 2013, **15**, 2104–2107.
- 54 T. Hasegawa, M. Sekine, W. P. Schaefer and H. Taube, Preparation and characterization of a bis(pentaammineosmium(II)) pyrene complex, *Inorg. Chem.*, 1991, **30**, 449–452.
- 55 H. Ito, K. Ozaki and K. Itami, Annulative  $\pi$ -Extension (APEX): Rapid Access to Fused Arenes, Heteroarenes, and Nanographenes, *Angew. Chem., Int. Ed.*, 2017, **56**, 11144–11164.
- 56 R. H. Martin and M.-J. Marchant, Thermal racemisation of [6], [7], [8] and [9] helicene, *Tetrahedron Lett.*, 1972, **13**, 3707–3708.
- 57 J. Barroso, J. L. Cabellos, S. Pan, F. Murillo, X. Zarate, M. A. Fernandez-Herrera and G. Merino, Revisiting the racemization mechanism of helicenes, *Chem. Commun.*, 2018, **54**, 188–191.
- 58 J. M. Fernández-García, P. Izquierdo-García, M. Buendía, S. Filippone and N. Martín, Synthetic chiral molecular nanographenes: the key figure of the racemization barrier, *Chem. Commun.*, 2022, **58**, 2634–2645.





- 59 G. Portella, J. Poater, J. M. Bofill, P. Alemany and M. Solà, Local Aromaticity of  $[n]$ Acenes,  $[n]$ Phenacenes, and  $[n]$ Helicenes ( $n = 1-9$ ), *J. Org. Chem.*, 2005, **70**, 2509–2521.
- 60 L. Rulišek, O. Exner, L. Cwiklik, P. Jungwirth, I. Starý, L. Pospíšil and Z. Havlas, On the Convergence of the Physicochemical Properties of  $[n]$ Helicenes, *J. Phys. Chem. C*, 2007, **111**, 14948–14955.
- 61 Y. Nakai, T. Mori and Y. Inoue, Theoretical and experimental studies on circular dichroism of carbo $[n]$ helicenes, *J. Phys. Chem. A*, 2012, **116**, 7372–7385.
- 62 P. Malakar, V. Borin, A. Bedi, I. Schapiro, O. Gidron and S. Ruhman, The impact of twisting on the intersystem crossing in acenes: an experimental and computational study, *Phys. Chem. Chem. Phys.*, 2022, **24**, 2357–2362.
- 63 K. Nagarajan, A. R. Mallia, K. Muraleedharan and M. Hariharan, Enhanced intersystem crossing in core-twisted aromatics, *Chem. Sci.*, 2017, **8**, 1776–1782.
- 64 J. B. Birks, D. J. S. Birch, E. Cordemans and E. Vander Donckt, Fluorescence of the higher helicenes, *Chem. Phys. Lett.*, 1976, **43**, 33–36.
- 65 H. Tanaka, Y. Inoue and T. Mori, Circularly Polarized Luminescence and Circular Dichroisms in Small Organic Molecules: Correlation between Excitation and Emission Dissymmetry Factors, *ChemPhotoChem*, 2018, **2**, 386–402.

